

Immune Activity and Response Differences of Oncolytic Viral Therapy in Recurrent Glioblastoma: Gene Expression Analyses of a Phase Ib Study



Katherine E. Miller^{1,2}, Kevin A. Cassady^{2,3}, Justin C. Roth⁴, Jennifer Clements⁵, Kathleen M. Schieffer¹, Kristen Leraas¹, Anthony R. Miller¹, Nripesh Prasad⁶, Jianmei W. Leavenworth^{5,7,8}, Inmaculada B. Aban⁹, Richard J. Whitley⁴, G. Yancey Gillespie⁵, Elaine R. Mardis^{1,2,10}, and James M. Markert⁵

ABSTRACT

Purpose: Previously, clinical trials of experimental virotherapy for recurrent glioblastoma multiforme (GBM) demonstrated that inoculation with a conditionally replication-competent $\Delta\gamma_{134.5}$ oncolytic herpes simplex virus (oHSV), G207, was safe. Following the initial safety study, a phase Ib trial enrolled 6 adult patients diagnosed with GBM recurrence from which tumor tissue was banked for future studies.

Patients and Methods: Here, we analyzed tumor RNA sequencing (RNA-seq) data obtained from pre- and posttreatment (collected 2 or 5 days after G207 injection) biopsies from the phase Ib study patients.

Results: Using a Spearman rank-order correlation analysis, we identified approximately 500 genes whose expression pat-

tern correlated with survival duration. Many of these genes were enriched for the intrinsic IFN-mediated antiviral and adaptive immune functional responses, including immune cell chemotaxis and antigen presentation to T-cells. Furthermore, we show that the expression of several T-cell-related genes was highest in the patient with the longest survival after G207 inoculation.

Conclusions: Our data support that the oHSV-induced type I IFN production and the subsequent recruitment of an adaptive immune response differed between enrolled patients and showed association with survival duration in patients with recurrent malignant glioma after treatment with an early generation oHSV.

Introduction

Glioblastoma multiforme (GBM) are central nervous system (CNS) tumors that are uniformly fatal with median survival of 12 to 15 months from initial diagnosis and 4 to 6 months after recurrence, despite all modalities of therapeutic intervention (1, 2). Standard of care, includ-

ing tumor resection, chemotherapy, and radiation currently offers limited survival benefit. The immunosuppressive microenvironment of GBM tumors contributes to this dismal prognosis (3–5). High-grade gliomas, including GBMs, express increased levels of immunosuppressive cytokines and demonstrate immune infiltrates that promote immune evasion and tumor progression (6, 7). Upon recurrence, GBMs commonly transition to a mesenchymal subtype characterized by even more enhanced immune suppression and a subsequent worse prognosis (8, 9). Designed to stimulate the immune system to attack tumor cells, immunotherapies are an evolving strategy for cancer treatment and have demonstrated remarkable responses in many malignancies. Oncolytic virotherapy, in particular, involves genetically engineered viruses designed to selectively replicate in tumor cells, relieving immunosuppression in the tumor microenvironment and enhancing antitumor immune responses.

Three phase I clinical trials investigated the safety of the oncolytic herpes simplex virus (oHSV), G207, in a cohort of 36 patients with recurrent GBM (10–12). As this was one of the first oHSVs tested in humans, the G207 trials were designed conservatively for safety. G207 lacks both copies of the $\gamma_{134.5}$ neurovirulence gene and contains a *lacZ* gene insertion that inactivates the viral ribonucleotide reductase (*U_L39* gene) and therefore has restricted replication *in vitro* and *in vivo* (10, 13). In a traditional 3+3 dose-escalation phase I trial, treatment was reported safe and produced no dose-limiting toxicities (10). Several G207-treated patients in this trial had impressive clinical responses: 2 subjects were long-term survivors (5.5 and 7.5 years in the pretemozolomide era), while a third subject died from an unrelated cause at 10 months post-G207 injection but had no viable tumor cells detected upon autopsy (10).

Following the initial safety study, a phase Ib trial enrolled 6 adult patients diagnosed with either GBM recurrence or progression.

¹The Steve and Cindy Rasmussen Institute for Genomic Medicine, Abigail Wexner Research Institute at Nationwide Children's Hospital, Columbus, Ohio. ²Department of Pediatrics, The Ohio State University College of Medicine, Columbus, Ohio. ³Center for Childhood Cancer and Blood Diseases, Abigail Wexner Research Institute at Nationwide Children's Hospital, Columbus, Ohio. ⁴Division of Pediatric Infectious Diseases, Department of Pediatrics, Heersink School of Medicine, The University of Alabama at Birmingham, Birmingham, Alabama. ⁵Department of Neurosurgery, Heersink School of Medicine, The University of Alabama at Birmingham, Birmingham, Alabama. ⁶HudsonAlpha Institute for Biotechnology, Heersink School of Medicine, Huntsville, Alabama. ⁷Department of Microbiology, The University of Alabama at Birmingham, Birmingham, Alabama. ⁸O'Neal Comprehensive Cancer Center, The University of Alabama at Birmingham, Birmingham, Alabama. ⁹Department of Biostatistics, School of Public Health, The University of Alabama at Birmingham, Birmingham, Alabama. ¹⁰Department of Neurosurgery, The Ohio State University College of Medicine, Columbus, Ohio.

K.E. Miller and K.A. Cassady are the co-first authors of this article.

Corresponding Author: James M. Markert, Department of Neurosurgery, Marnix E. Heersink School of Medicine, The University of Alabama at Birmingham, 1060 Faculty Office Tower, 510 20th Street South, Birmingham, AL 35233. Phone: 205-934-7170; E-mail: jmarkert@uabmc.edu

Clin Cancer Res 2022;28:498–506

doi: 10.1158/1078-0432.CCR-21-2636

This open access article is distributed under the Creative Commons Attribution-NonCommercial-NoDerivatives 4.0 International (CC BY-NC-ND 4.0) license.

©2022 The Authors; Published by the American Association for Cancer Research

Translational Relevance

Oncolytic virotherapy is an evolving treatment strategy for many types of malignancies and is gaining traction in several research and clinical settings. The increasing use of virotherapy in clinical trials offers the unprecedented opportunity to perform molecular studies on tumor tissue before and after treatment. Here, we use RNA sequencing and gene expression panels to identify transcriptomic differences in recurrent glioblastoma multiforme following virotherapy with G207 in a phase I trial. Our data suggest that IFN production, the ensuing recruitment of an adaptive T-cell immune response, and detection of G207 viral transcripts 5 days after injection were associated with overall survival duration in our cohort of patients. Altogether, our findings demonstrate the variability in immune response in different patients after virotherapy and elucidate immune transcript changes that likely are associated with a more successful response to antitumor oncolytic virotherapy.

Following surgical resection but prior to oHSV injection, all patients received radiotherapy and all but 1 patient received chemotherapy. Patients were then treated twice with G207—an initial intratumoral stereotactic injection of the virus, followed 2 or 5 days later by an *en bloc* resection and infusion of the virus again into the resection cavity (Fig. 1A) (11). The phase Ib trial demonstrated safety in administering multiple oHSV doses into the brain including into the resection cavity. Analyses of resected tumor tissue including IHC staining and PCR of viral genes revealed marked cytotoxic lymphocyte infiltration and the presence of HSV DNA, respectively, indicating an active antitumor response. Overall, the highly attenuated G207 modestly extended median survival (6.6 months). Survival varied between patients with 1 patient deriving no discernable benefit from virotherapy (60 days survival post-G207) and another living for 21 months after G207 therapy.

In this study, we sought to identify biological differences that could elucidate the variable survival duration associated with G207 virotherapy. A summary of patient demographics, tumor subtype, survival, and analyses performed in this study are shown in Fig. 1B. We generated RNA sequencing (RNA-seq) from pre- and post-G207 treatment tumor biopsies to investigate changes in gene expression during the treatment interval. Based upon our previous IHC analyses demonstrating cytotoxic immune cell infiltrates in some long-term survivors, we hypothesized that gene expression indicative of an active immune response would be characteristic of patients with improved survival (11).

Patients and Methods

Clinical trial specimens

We obtained fixed tumor specimens from the phase Ib G207 clinical trial (NCT00028158), in accordance with institutional review board (IRB) approval. GBM subtypes for each tumor were defined based on analysis of microarray data to assign subtypes at the time of initial diagnosis, more than 10 years ago.

RNA extraction, library preparation, and sequencing

RNA was extracted using Covaris truXTRAC formalin-fixed, paraffin-embedded (FFPE) total nucleic acid kit. For pre-G207 samples, RNA was subjected to DNase treatment and ribodepletion using Illumina TruSeq Stranded total RNA kit; paired-end 151 bp reads

were generated on Illumina HiSeq 4000. For post-G207 samples, RNA libraries were prepared using Illumina TruSeq stranded mRNA kit; paired-end 50 bp reads were generated on Illumina GAIIx.

RNA-seq data processing, visualization, and differential expression

We generated normalized expression values [transcript per million (TPM) values] as follows: FASTQ files were used as input for Salmon in mapping-based mode using human reference transcriptome RefSeq GRCh38 (14). We used standard Salmon parameters with bootstrapping set to 100. Gene-level TPMs were generated using *tximport* (15). When indicated, we filtered genes for gene type “protein_coding” and used the resulting genes for downstream analyses (16). For principal component analysis (PCA), the top 500 most variable genes were identified using rowVars from *matrixStats* R package and then evaluated by unsupervised two-dimensional PCA using the R stats function *prcomp* (17). We used *heatmap* R package for unsupervised hierarchical clustering. CIBERSORT was used to predict immune cell abundance from RNA-seq data; TPM expression values and the provided LM22 gene expression signature matrix were used as input for absolute mode with parameters set to 1,000 permutations and quantile normalization disabled before processing (18). Differential gene expression analysis was performed using *DESeq2* R package with longest term survivor compared with a reference group composed of other responders (PT103 and PT105) who survived longer than the average 150 days expected for a diagnosis of recurrent GBM (19).

Functional annotation and pathway analysis

Significant genes identified in our Spearman correlation analysis were used for functional annotation analysis using The Database for Annotation, Visualization, and Integrated Discovery (DAVID) version 6.8 and for pathway analysis using Qiagen Ingenuity Pathway Analysis (IPA) software (20). For IPA analysis input, we included *P* values from our Spearman analysis as well as fold changes (FC) for each gene; FCs were calculated using TPM from the longest survivor (PT107) divided by average TPM from the two shortest term survivors (PT101 and PT108).

NanoString gene expression profiling and cell-type prediction

Multiplexed gene expression profiling was performed using the PanCancer Immune Profiling Panel (version 1.1) from NanoString Technologies. Tumor-extracted RNA (150 ng) was prepped according to manufacturer’s protocol. Data were normalized using housekeeping genes noted within the panel and analyzed using the advanced analysis module of nSolver software. The advanced analysis module uses a previously published method to measure the abundance of various cell populations, using marker genes which are expressed stably and specifically in given cell types (21). These values are referred to as cell type “scores” throughout our manuscript.

IDH1 p.R132 and IDH2 p.R172 high-depth sequencing

Tumor DNA (1–10 ng) was used as a template for PCR. Isocitrate dehydrogenase 1 (*IDH1*) p.R132 primers (GRCh38): forward (5'-ACCTTGCTTAATGGGTGTAGAT-3') and reverse (5'-CTGCAAAAATATCCCCCGGC-3') and Isocitrate dehydrogenase 2 (*IDH2*) p.R172 primers (GRCh38): forward (5'-CAGAGACAAGAGGATGGCTAGG-3') and reverse (5'-TTCCGGGAGCCCATCACTG-3'). PCR was performed using 2x Q5 MM (New England BioLabs) and 200 nmol/L primers with the following conditions: 30'' at 98°C, 30 cycles of 10'' at 98°C, 20'' at 58°C, 20'' at 72°C, and

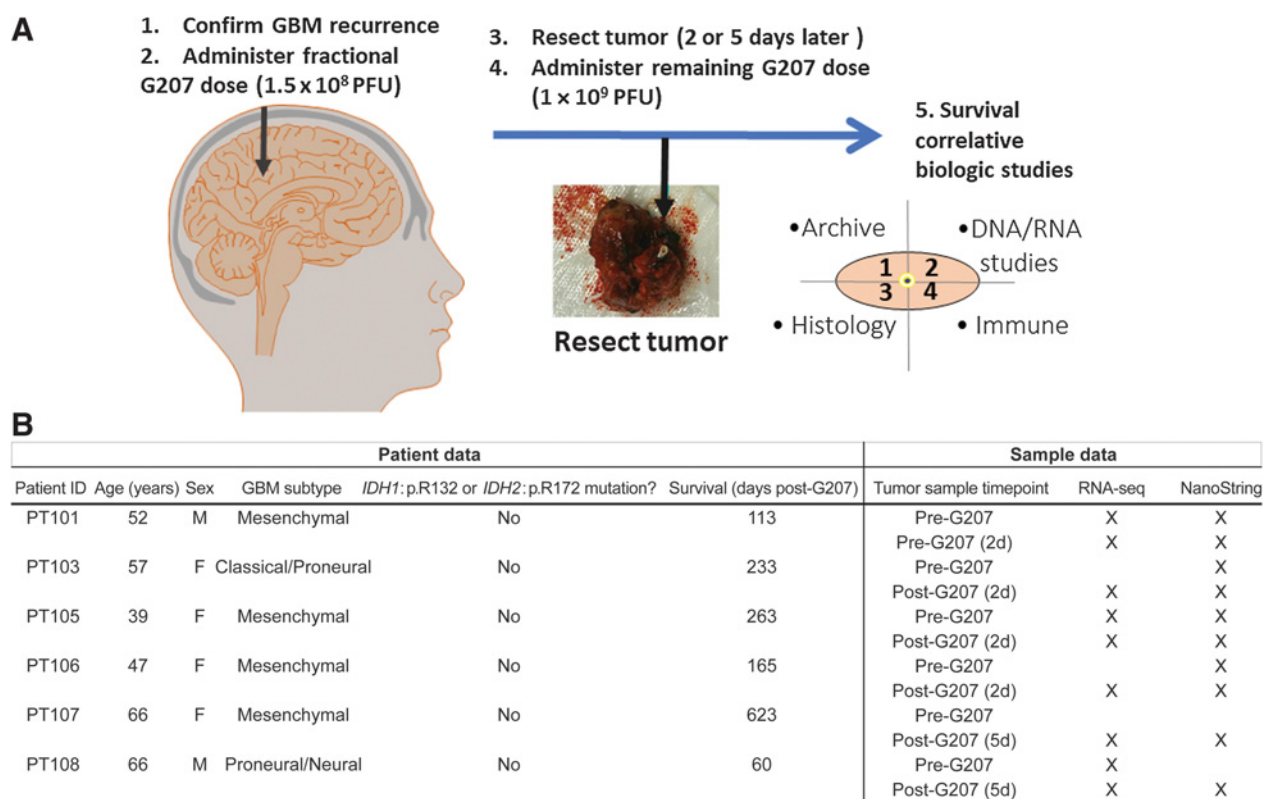


Figure 1. Overview of the G207 clinical trial design and patient demographics. **A**, Phase Ib-enrolled patients were treated with a fractional G207 dose [15% of the recommended phase II dose (RP2D)] after biopsy confirmation of malignant GBM recurrence based on histopathology. Patients then underwent tumor resection 2 or 5 days later and had the remaining G207 RP2D dose injected into the margins of the resection cavity. The resected G207-treated tumor samples were then divided and analyzed as shown in the schematic. Our manuscript focuses specifically on RNA studies. **B**, Summary of patient clinical trial identifiers, GBM tumor subtype, *IDH1/2* hotspot mutational status, survival post-G207 treatment (in days), and available samples for our study. Timepoint of when the sample was taken is shown as 2 or 5 days ('d') post-treatment. "X" indicates available data for RNA-seq and/or NanoString gene expression assays. PFU, plaque-forming units.

a final extension of 5' at 72°C. Amplified products were purified using 1.8X SPRIselect and then amplified for an additional 30 cycles followed by end-repair and dA-tailing using NEBNext Ultra II DNA Library Prep kit reagents. The reaction was followed by adapter ligation with unique molecular identifier-Integrated DNA Technologies (UMI-IDT)-indexed adaptors. Adaptor-ligated samples were purified using 1.0X SPRIselect followed by 0.9X SPRIselect and used for library amplification with Q5 MM and Illumina P5/P7 primer mix. A post-PCR 1.2X SPRIselect clean-up was performed, and libraries were pooled and sequenced on iSeq100 to achieve high-depth sequencing coverage more than 4,500X.

Statistical analysis

We calculated Spearman rank-order correlation coefficients as follows—for each gene, we calculated rank of TPM values for each sample and calculated rank for patient survival (measured in days posttreatment, i.e., 1 = longest survival and 6 = shortest survival). We then calculated Spearman rank-order correlation for each gene using TPM rank compared with survival duration in all 6 patients. A two-tailed *t* test was performed using calculated *t* values for each correlation value [$t = \sqrt{((r^2 * df)/(1 - r^2))}$, where *df* is degrees of freedom = 4] and the TDIST function in Microsoft Excel. We then filtered by $P \leq 0.05$ to get a final set of genes ($n = 502$) for analyses. Significance testing

Table 1. Top gene ontology terms associated with G207-induced gene expression changes.

Term	FDR ^a	Count ^b	% ^c
Immune response	4.80E-09	28	12.0
Neutrophil chemotaxis	3.80E-07	12	5.1
Chemokine-mediated signaling pathway	5.80E-07	12	5.1
Monocyte chemotaxis	1.50E-05	9	3.8
Inflammatory response	9.00E-05	20	8.5
Antigen processing and presentation	9.20E-05	9	3.8
Lymphocyte chemotaxis	2.20E-04	7	3.0
Cell chemotaxis	2.60E-04	9	3.8
Chemical synaptic transmission	3.30E-04	15	6.4
Positive regulation of inflammatory response	5.00E-04	9	3.8
Cellular response to IFN γ	8.70E-04	8	3.4

Note: The top 500 most variable genes identified through RNA-seq analysis were uploaded to the DAVID. The most significant biological processes associated with the 500 identified genes are displayed in the table.

^aFDR, Benjamini FDR.

^bCount, number of genes in our uploaded dataset of 500 that match with number of genes for that biological process.

^cPercentage of genes in our uploaded dataset that match with number of genes for that biological process.

Table 2. Biological processes which correlate with survival in post-G207 samples are associated with immune response.

ID ^a	Term	FDR ^b	Count ^c	% ^d
GO:0006955	Immune response	2.08E-14	35	14.7
GO:0042110	T-cell activation	6.84E-07	11	4.6
GO:0032496	Response to lipopolysaccharide	8.04E-07	17	7.1
GO:0002250	Adaptive immune response	1.26E-04	14	5.9
GO:0006954	Inflammatory response	2.28E-04	21	8.8
GO:0050776	Regulation of immune response	6.79E-03	13	5.5
GO:0031295	T-cell costimulation	1.36E-02	9	3.8
GO:0045060	Negative thymic T-cell selection	1.46E-02	5	2.1
GO:0050852	T-cell receptor signaling pathway	4.25E-02	11	4.6
GO:0032715	Negative regulation of IL6 production	4.71E-02	6	2.5
GO:0032088	Negative regulation of NF-κB transcription factor activity	6.53E-02	8	3.4
GO:0030816	Positive regulation of cAMP metabolic process	7.15E-02	4	1.7
GO:0007166	Cell surface receptor signaling pathway	1.14E-01	14	5.9
GO:0042130	Negative regulation of T-cell proliferation	1.89E-01	6	2.5
GO:0010818	T-cell chemotaxis	1.96E-01	4	1.7
GO:0032720	Negative regulation of tumor necrosis factor production	2.16E-01	6	2.5
GO:0019835	Cytolysis	2.39E-01	5	2.1
GO:0006935	Chemotaxis	3.39E-01	9	3.8
GO:0007169	Transmembrane receptor protein tyrosine kinase signaling pathway	4.43E-01	8	3.4
GO:0070098	Chemokine-mediated signaling pathway	5.51E-01	7	2.9

Note: Genes with significant *P* values in our Spearman rank-order analysis were uploaded into the DAVID database. The top 20 results sorted by decreasing FDR *P* value are displayed.

^aID, GO database identifier.

^bFDR, Benjamini FDR.

^cCount, number of genes in our uploaded dataset of 500 that match with number of genes for that biological process.

^dPercentage of genes in our uploaded dataset that match with number of genes for that biological process.

between cell types (displayed in **Fig. 3B**) was performed using an unpaired, two-sided *t* test. Adjusted *P* values in **Tables 1** and **2** are Benjamini FDR and were output from DAVID. Adjusted *P* values in **Table 3** are Benjamini FDR and were output from DESeq2.

Data availability statement

The RNA-seq and NanoString gene expression data presented in this publication have been deposited in NCBI's Gene Expression Omnibus (GEO) and are accessible through GEO Series accession number GSE164105 (<https://www.ncbi.nlm.nih.gov/geo/query/acc.cgi?acc=GSE164105>).

Results

As shown in **Fig. 1**, 6 patients underwent tumor resection 2 (PT101, PT103, PT105, PT106) or 5 days (PT107 and PT108) after receiving the first of two inoculations of G207. Most patients (PT101, PT105, PT106,

Table 3. Differentially expressed genes in patient with longest survival versus all other responders are associated with antigen presentation and cytotoxic response.

Gene	Immune function	Log ₂ FC	FDR ^a
<i>CCL13</i>	Chemotactic factor that attracts monocytes, lymphocytes, basophils, and eosinophils	6.97	0.000
<i>IL2RA</i>	Constitutively expressed in resting memory T cells	4.52	0.000
<i>FOSB</i>		3.36	0.000
<i>CIQTNFI</i>		3.46	0.000
<i>GFAP</i>		-3.07	0.000
<i>MMP12</i>		5.87	0.003
<i>IGFBP6</i>		3.55	0.008
<i>CLEC4G</i>	Plays a role in the T-cell immune response and viral entry into cell	4.17	0.030
<i>CHAT</i>		6.69	0.038
<i>CXCL9</i>	Chemotactic for activated T cells; binds to CXCR3	3.76	0.053
<i>POSTN</i>		3.83	0.064
<i>CALB1</i>		3.50	0.064
<i>COL13A1</i>		3.20	0.064
<i>TRH</i>		4.59	0.098
<i>ADAMTS9</i>		2.16	0.098
<i>COL19A1</i>		3.13	0.128
<i>SIK1</i>		3.59	0.130
<i>HLA-DQA1</i>	Antigen presentation/processing	2.69	0.130
<i>TIMD4</i>	Involved in regulating T-cell proliferation and lymphotoxin signaling	3.40	0.204
<i>GZMB</i>	Secreted by NK cells and CTLs and proteolytically processed to generate the active protease, which induces target cell apoptosis	2.79	0.204
<i>CD8A</i>	Found on most CTLs; T-cell coreceptor	2.61	0.207
<i>FAM110C</i>		2.74	0.223
<i>HMG2</i>		3.37	0.227
<i>LDLR</i>		1.82	0.231
<i>STUM</i>		-1.88	0.231
<i>ITK</i>	Encodes an intracellular tyrosine kinase expressed in T cells; thought to play a role in T-cell proliferation and differentiation	2.71	0.236
<i>FAM46C</i>	May be involved in induction of cell death	2.35	0.236
<i>HMOX1</i>		2.19	0.236
<i>THBS1</i>		1.57	0.239
<i>COL5A1</i>		1.62	0.242

Note: Differential expression analysis was performed using DESeq2 to compare the patient with longest survival post-G207 (PT107) versus all other responders. Genes with FDR ≤ 0.25 are displayed. Immune function(s) for each gene, if any, are displayed and were curated manually from both Entrez gene and UniProtKB/Swiss-Prot summaries.

^aFDR, Benjamini FDR.

PT107) had a mesenchymal GBM while 2 patients (PT103, PT108) had a classical/proneural subtype. Tumors were genotyped for *IDH1*:R132 and *IDH2*:R172 mutations, but no driver mutations were detected in any samples. To identify whether certain gene expression changes correlated with virotherapeutic response and improved survival, we analyzed tumor-extracted RNA via RNA-seq. We also evaluated the immune-specific expression profiles as a proxy for estimating types and abundance of infiltrating immune cells using a predesigned commercially available gene expression panel (PanCancer Immune Profiling Panel, NanoString Technologies, Inc.).

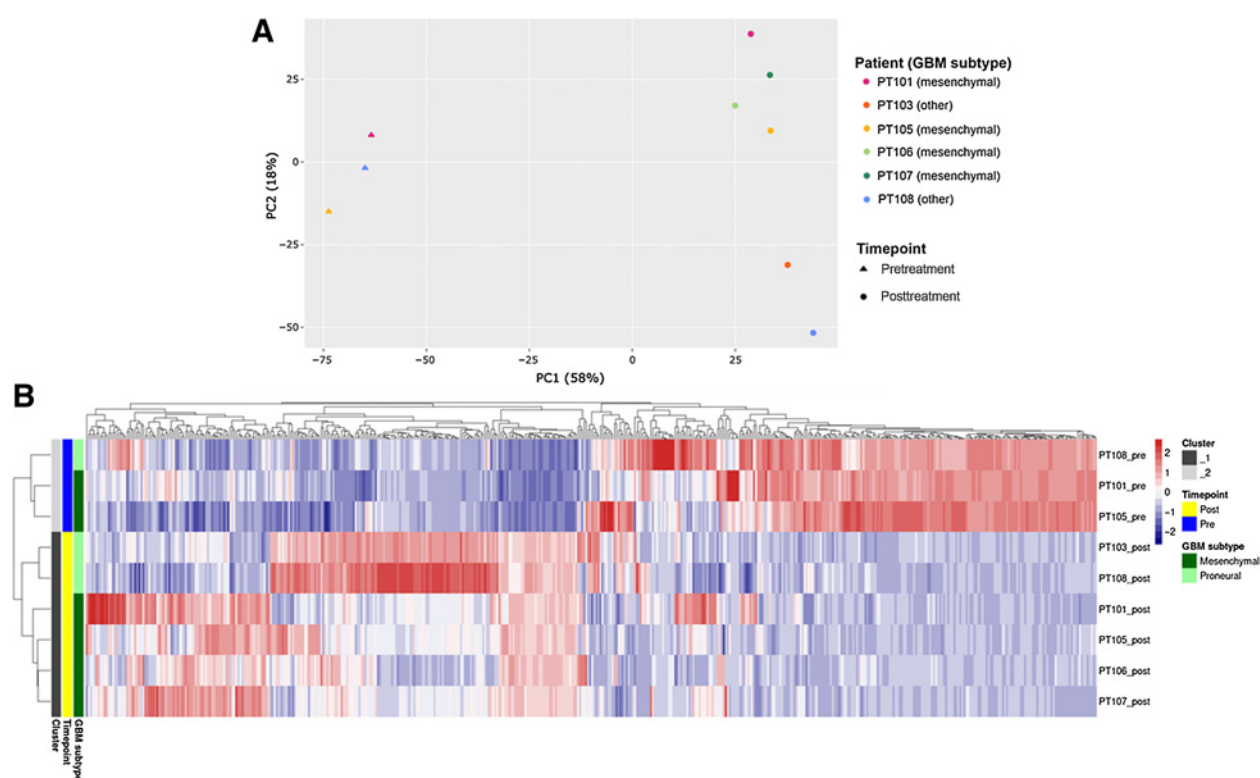


Figure 2.

PCA and hierarchical clustering of RNA-seq gene expression values is driven by G207 treatment in pre- and posttreated biopsies. **A**, The top 500 most variable protein-coding genes were used to perform unsupervised PCA. Samples are colored by clinical trial identifiers while shapes designate timepoint relative to G207 treatment. **B**, Unsupervised hierarchical clustering of RNA-seq expression values, using the topmost 500 variable genes between all samples. Each column represents a gene, while rows represent individual samples. Color legend represents the \log_2 calculated relative expression scaled per column (gene). Sample annotations are displayed on left and include cluster ID (based on hierarchical clustering), treatment timepoint (pre- or post-G207), and GBM tumor subtype.

Gene expression differences in pre- versus post-G207-treated tumor specimens

We first compared pre- and post- G207 treatment RNA-seq using unsupervised PCA. The PCA results clearly segregated pre- and posttreatment groups with a PC1 separation of 58% (Fig. 2A). G207 treatment had a greater impact on gene expression-based sample clustering than did GBM subtype (PC2; 18%, Y axis Fig. 2A). Similarly, unsupervised hierarchical clustering separated the samples into two distinct clusters, indicating that G207 virotherapy was the primary driver of transcriptome-based clustering (Fig. 2B).

Next, we sought to determine any biological functions associated with the post-G207 treatment gene expression cluster. We performed Gene Ontology (GO) analysis using the PC1 component genes. As shown in Table 1, our analysis revealed that genes enriched in G207-treated samples characterized biological processes involving immune response, including immune cell recruitment, antigen processing and presentation, and positive regulation of the inflammatory response. GO classification by “molecular function” revealed significant association with chemokine activity while pathway mapping using GO analysis and the Kyoto Encyclopedia of Genes and Genomes (KEGG) database revealed enrichment for cytokine and chemokine signaling pathways (Supplementary Table S1).

We further characterized RNA extracted from pre- and post- G207-treated samples by multiplex gene expression analysis focusing on a panel of 770 immune response genes representing 24 different immune cell types (PanCancer Immune Panel). Again, PCA analysis

with this data revealed that G207 treatment, more than any other component including GBM subtype, had the greatest effect on immune gene expression changes (PC1 = 41%; Supplementary Fig. S1A). Similar to the RNA-seq analysis described above, unsupervised hierarchical clustering using the PanCancer immune gene expression data revealed two distinct clusters of pre- and posttreatment samples (Supplementary Fig. S1B).

We then examined which immune cell types in particular were enriched in the post-G207 samples. Here, 109 marker genes specific to 24 major immune-cell populations were used to assign “cell type scores” (see methods). Nearly all post-G207 samples have higher abundance of immune cells relative to pre-G207 samples (Fig. 3A). Specifically, G207 treatment significantly increased the cytotoxic, T-cell, natural killer (NK and NK-CD56dim), macrophage, neutrophil, and dendritic cell (DC) scores (Fig. 3B). In addition to comparing the individual cell type absolute scores that changed significantly post-G207, we also compared the relative immune cell scores, measured as a proportion of total immune score (Fig. 3C). These results indicated G207 reduced the proportion of infiltrating exhausted T-cells, in that the largest change was the ratio of exhausted T-cells to total tumor-infiltrating lymphocytes (TIL; Fig. 3C). The greatest relative changes following G207 treatment involved an increased proportion of T-cells (CD4 and CD8), CD8⁺ T-cell to exhausted CD8⁺ T-cell ratio, and the NK CD56 dim to total TIL ratio. These results also demonstrated that T-cell:TIL and DC:TIL ratios increased following G207 treatment, and that the exhausted cytotoxic T-cell

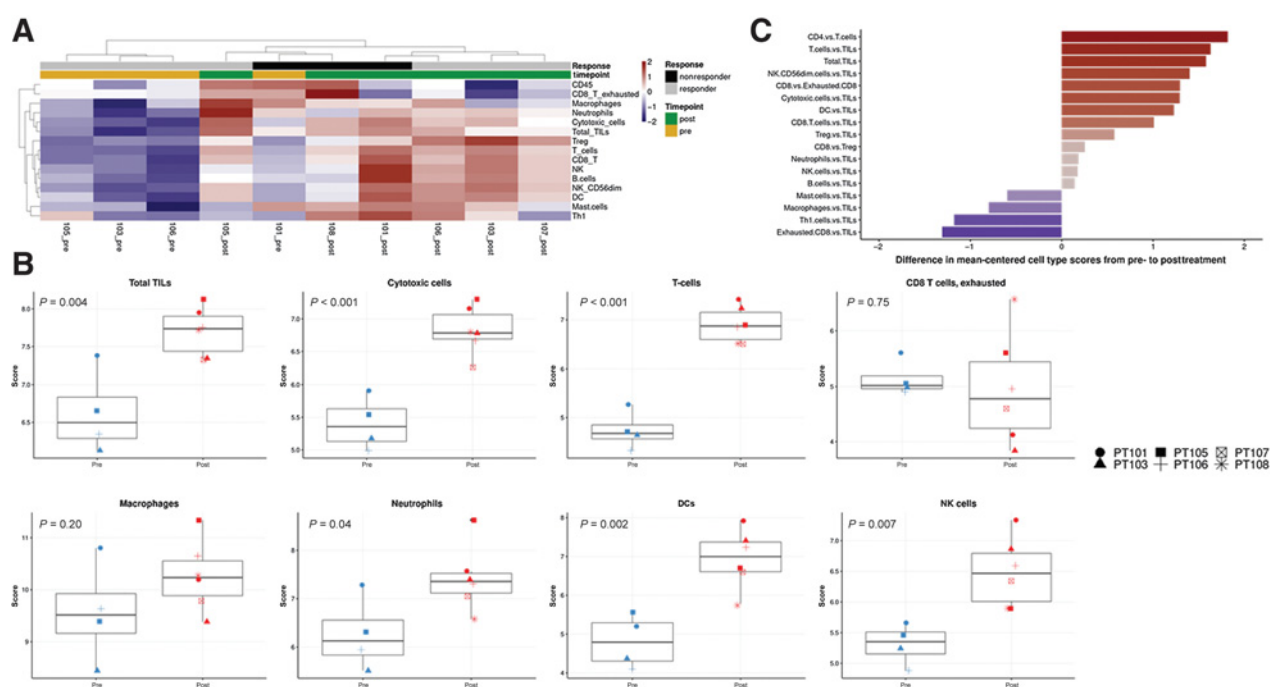


Figure 3. Immune cell type scores using PanCancer gene expression panel are higher in post-G207 versus pre-G207 samples. **A**, Heatmap displaying immune cell types (rows) and samples (columns). Annotations for treatment timepoint and response are displayed as colors at top. Relative abundance of cell types is estimated based on marker genes identified in PanCancer immune panel for each sample, and values are scaled per row. “Responders” are defined as patients who survived beyond the median survival of 150 days. **B**, Boxplots for specific immune cell type measurements against timepoint (blue = pre-G207, red = post-G207) are shown. Cell type measurements are derived from expression of marker genes in the PanCancer immune panel (see Methods). “Total TILs” score was calculated as the average of all cell type scores whose correlations with CD45 exceeded 0.6. *P* values were calculated using an unpaired, two-sided *t* test. **C**, Cell type scores in post-G207 samples relative to pre-G207 samples. Displayed is the difference in mean-centered cell type scores for each cell type, shown as the difference in post-G207 relative to pre-G207. Red indicates values for post-G207 treatment while blue indicates values for pre-G207 treatment. CD45, CD45-positive cells.

population relative to TIL score declined. Our analysis also showed relatively minor changes in the CD8 to T-regulatory cells and T-regulatory cells to TIL ratios when comparing pre- and post-G207 treatment data.

Next, RNA-seq results from the pre- and post- G207 treatment samples were analyzed using CIBERSORT-based deconvolution. CIBERSORT scores indicated that PT107 (best responder, as defined by longest survival following G207 treatment) had the highest proportion of TILs post-G207 treatment. In particular, PT107 had a higher proportion of memory CD4 T cells, CD8 T-cells, and macrophages compared with all other patients. PT108 (worst responder, as defined by shortest survival following G207 treatment) had the lowest infiltration of TILs present in the posttreatment biopsy (Supplementary Fig. S2A). We sought to validate deconvolution results orthogonally using two additional algorithms: quanTIseq and xCell via TIMER2.0 web server (22–24). The additional algorithms yielded similar predictions in that PT107 post-G207 had higher CD8 T-cells than any other sample (Supplementary Fig. S2B).

Correlation analysis of gene expression and survival duration

We sought to test our hypothesis that immune expression changes enriched in post-G207 treatment RNA were associated with survival following treatment. Median survival of GBM recurrence is 4 months (150 days), and while 4 of 6 G207-treated patients from the phase Ib study survived longer than this, their survival duration was quite variable (Fig. 1B).

We tested whether there was a direct correlation between the post-G207 treatment gene expression levels (TPM) and survival (days) using a Spearman rank-order correlation analysis. Our goal was to identify genes associated with oHSV antitumor response in terms of overall survival (OS; Fig. 4A) and to assess whether these genes were enriched for treatment-related biological or immune functions. Our initial Spearman correlation analysis identified 502 protein-coding genes that directly correlated with OS (Fig. 4B; for the full list see Supplementary Table S2A). IPA analysis revealed over half of these “survival-related” genes participate in immune response pathways (Table 2 and Fig. 4C). When we identified upstream regulatory pathways in IPA using the same set of 502 genes, both the intrinsic antiviral response (pattern recognition receptor activation of a type I IFN response) and adaptive immune response (T-cell & NK-cell stimulatory cytokine production—*IL21*, *IL27*, *IL12*, *IFN γ*) correlated with OS (Supplementary Fig. S3). IPA regulatory effect analysis of the Spearman significant genes revealed the top regulatory networks regulate immune cell chemotaxis (mononuclear and lymphocytic) and antigen presentation to T-cells (Supplementary Fig. S4).

As expected, most enrolled patients (4 of 6) in the phase Ib clinical trial harbored the more common mesenchymal subtype of GBM based on microarray analysis. The patient with the longest survival duration post-G207 (PT107) had a mesenchymal GBM whereas the patient with the shortest survival post-G207 (PT108) had a proneural GBM. We sought to identify whether differences between GBM subtypes biased our initial gene expression findings. Therefore, we reanalyzed only the 4 patients with mesenchymal GBMs using the same Spearman

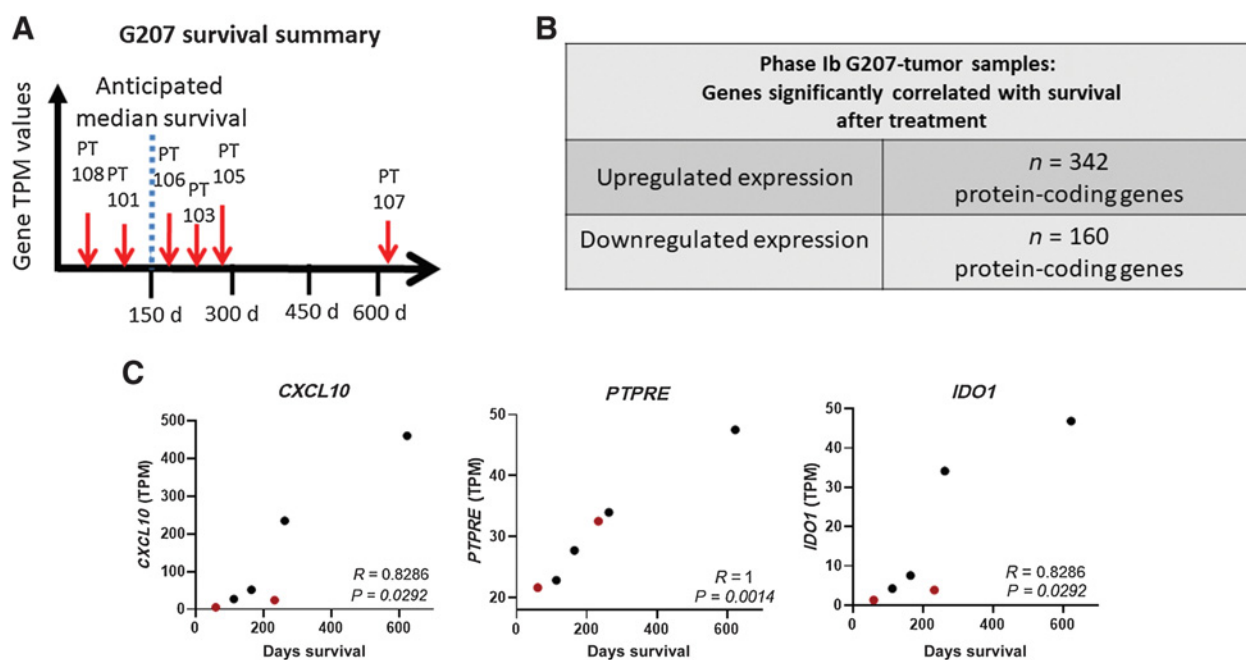


Figure 4.

Spearman correlative analysis reveals significant set of genes associated with patient survival. **A**, Schematic correlative approach (TPM per gene vs. days of survival). **B**, Summary of the significant genes whose Spearman P values were ≤ 0.05 . The full list of genes can be found in Supplementary Table S2A. **C**, Example of three of the 502 genes analyzed and their relationship between gene expression and survival; black dots represent mesenchymal tumors while red dots represent proneural or other subtype.

correlation approach described above and identified 655 genes ($P \leq 0.05$) that directly correlated with survival (Supplementary Table S2B). Of these survival-related genes in the mesenchymal subset, 165 overlapped with our Spearman gene list from our entire cohort (Supplementary Table S2C). IPA analysis of the overlapping genes ($n = 165$) revealed an association with immune functions including T-cell chemotaxis, recruitment of lymphocytes, and immune-cell migration in these tumors (Supplementary Fig. S5). The remaining survival-related genes ($n = 490$) did not overlap with the larger cohort survival genes and were unique to the mesenchymal subgroup. These genes, upon IPA analysis, were associated with neuronal and metabolic signaling pathways but not with any immune-related pathways (Supplementary Table S3). These results suggest OS correlated with immune response to oHSV treatment and was not related to an immune response unique to the mesenchymal subgroup that potentially biased our survival analysis.

Identification of immune-specific genes enriched in the patient with longest survival following G207 treatment

This analysis compared gene expression and pathway analysis differences between PT107 and other responders, defined by a survival time of longer than 4 months following G207 administration. We sought to identify differentially expressed genes in PT107 that might explain their extraordinary response (623 days survival post-G207). Using DESeq2, a total of 15 significant ($|\log_2FC| > 2$ and $FDR \leq 0.1$) differentially expressed genes were identified between PT107 compared with all other responders (Table 3). Several of the overexpressed genes in PT107 relative to other responders, including *CCL13*, *IL12RA*, *CXCL9*, *GZMB*, and *HLA-DQA1* are associated with recruitment of T-cells and other lymphocytes, antigen presentation, and apoptosis.

Discussion

The first replication competent oHSV we tested in humans, G207, was conservatively designed for safety and therefore replicated poorly (25). Yet, it had demonstrable antiglioma effects, including improved survival in some patients. The results of these trials showed that an oHSV: (i) could be safely injected into the brains of patients with GBM, (ii) could be safely injected repeatedly, and (iii) did not produce dose-limiting toxicities.

Using next-generation RNA-seq techniques and other gene expression assays, our studies identified biological pathways that illustrate differences in immune-mediated responses to virus treatment as a function of the duration of survival across patients. We detected approximately 500 genes that significantly correlated with patient survival and demonstrated that approximately 50% of these genes were related to immune response pathways and functions. Network IPA analysis and RNA-seq deconvolution of immune-cell populations after treatment with oHSV revealed associations with patient survival and identified important mechanistic events related to cellular infiltrate changes including an increase in the myeloid, cytotoxic, and T-cell populations, suggesting a relationship between immune gene response and survival duration. Previously published data from this clinical trial cohort examined CD4 and CD8 infiltrate primarily but did not examine potential immune function response differences on a more global scale between samples (11). The original studies examining PT107 (best responder) IHC staining of CD3 or CD8 described limited changes to the infiltrate. However, we speculate that for the tumor sections, heterogeneity plus proximity to the injection site could pose bias when performing IHC on a single tumor section. Our current RNA-based analyses sample an entire paraffin-embedded section of tumor tissue and therefore offer an

integrated analysis from the entire biopsy sample. Our gene expression analyses provide a more nuanced interpretation of immune-cell and tumor-associated gene expression changes over the entirety of the tumor section and a snapshot of the bulk RNA profile of the tumor resected after oHSV injection.

Our results do not exclude the possibility that the improved immune response could be related to viral gene expression. The previous publication at the time of the clinical trial demonstrated RNA copies of HSV polymerase were detected at the highest amounts from the best responder (PT107) but that viral DNA copies were similar between all the treated patients (11). Similarly, we performed metagenomic alignment of RNA-seq data from post-G207 samples and identified G207 (α herpes virus) transcripts present only in PT107 but no other samples (Supplementary Table S4). Other patients in this study, however, had survival durations beyond the median survival expected for GBM recurrence and had immune activation identified in gene expression pattern changes, indicating our analyses show immune response changes independent of viral activity.

Of particular interest to the clinical implications for our research is how these results should impact our ongoing immunotherapy and oncolytic virotherapy trials. The gene sets identified permit further interrogation of gene expression response predictors when evaluating the impact of different recombinant oncolytic viruses. Currently, there are numerous active oncolytic viral clinical trials ongoing, five of which involve the treatment of CNS tumors using recombinant herpes virus vectors of various designs [ClinicalTrials.gov; search term: (oncolytic) AND (virotherapy OR viral therapy) AND (herpes simplex virus OR HSV) and then manually filtered for “conditions” of brain tumor]. We anticipate that similar evaluative approaches to clinical trial samples will identify mechanisms that are integral to oncolytic virotherapy efficacy and will further inform future studies. Current results from preclinical models suggest that early viral replication, IFN induction, T-cell stimulatory activity, and shifts in macrophage polarization, activation, and antigen presentation are integral to oHSV therapeutic success (26–30). In addition, there are preclinical data indicating that early NK-cell activity during the first few hours following viral treatment can limit the initial viral burst, potentially limiting the ensuing myeloid and adaptive responses (31–34). Our G207 clinical trial gene expression analyses support each of these results and, taken together, demonstrate the complexity of the immune-mediated response after virotherapy and the importance of monitoring for these responses.

The study has certain limitations, the most notable being the limited numbers of patient samples available for analysis. We studied pre- and posttreatment samples from 6 patients with nine samples (3 pre-G207 and 6 post-G207) available for RNA-seq and ten samples (4 pre-G207 and 6 post-G207) for NanoString gene expression assay. Even without pretreatment samples for all 6 patients, we demonstrated that immune gene expression was higher in post-G207 samples relative to the pre-G207 samples available (as displayed in Figs. 2 and 3). To further demonstrate that GBMs prior to any immunotherapy have low immune infiltration at baseline, we analyzed RNA-seq data from The Cancer Genome Atlas (TCGA) and other datasets available through the GEO (35). The fraction of GBM tumors predicted to have significant immune infiltration was lower than any other brain cancer and as expected, was lower than other extracranial solid tumors; furthermore, the fraction of those immune cells predicted to be CD8 T-cells was approximately 2% (Supplementary Table S5). These analyses support our manuscript results that the overexpression of CD8 T-cell transcripts (and therefore inference of infiltration of CD8 T-cells) are relatively low in GBMs at baseline and the increase is likely due to the G207 treatment in our patients. Other studies have previously demonstrated via RNA-

seq, immunofluorescent staining, and flow cytometry that recurrent GBMs had low representation of immune infiltration—particularly low in IFN- and T-cell-related pathways, like what we observed in our pre-G207-treated tumors (36, 37). Finally, in a recent report from NCT02457845, a phase I clinical trial to determine the safety of injecting G207 into pediatric recurrent high-grade gliomas, the authors demonstrated few immune-related cells in the initial core biopsies prior to G207 treatment via IHC staining for CD8 (38).

Taken together, our transcriptional analyses demonstrate that treatment with the oHSV G207 in recurrent GBMs significantly shifted tumor-associated gene expression and profoundly altered the intratumoral cellular immune populations and their activities. One patient had an extraordinary clinical response, almost 2-year survival after treatment of recurrent GBM, that corresponded with these posttreatment immune-related sequelae which included higher expression of many T-cell- and IFN-related genes. Using RNA-seq and gene expression data, our analysis suggests that responsive patients exhibited increase in genes involved in antigen presentation as well as improved cytotoxic and T-cell adaptive immune activity following virotherapy, all of which corresponded with improved survival.

Authors' Disclosures

K.A. Cassady reports licensure payments from Mustang Bio for the C134 virus but there are no relevant financial conflicts for the technology addressed in this manuscript. J. Clements reports grants from NIH NCI during the conduct of the study. I.B. Aban reports grants from Verona Pharmaceutical, Myasthenia Gravis Foundation (MGFA) of America, Ra/UCB Pharmaceutical, Alexion, Argenx, and Catalyst outside the submitted work. G.Y. Gillespie reports grants from USPHS and NCI during the conduct of the study and other support from Aettis, Inc. and Treovir, LLC outside the submitted work. E.R. Mardis reports personal fees and other support from Qiagen N.V., PACT Pharma LLC, and Scorpion Therapeutics LLC outside the submitted work. J.M. Markert reports grants from NIH, Department of Defense, Geteway, NIH and other support from Medigene, Inc. during the conduct of the study; other support from Aettis, Inc., Treovir, Inc., LLC, Amgen, Inc., Merck, and Imugene, Ltd and nonfinancial support from Mustang Bio Tech outside the submitted work; in addition, J.M. Markert has a patent 6764675 issued, a patent for UAB-16102/22 pending, a patent for DRU-2019-7123 issued, a patent for 62/824,685 pending, and a patent for WO 2020/198680 A1 pending; and Orphan Drug Designation, M032 Oncolytic HSV, IND#14946 for oncolytic HSV M032, and IND #17296 for oncolytic HSV C134 (J.M. Markert is sponsor-investigator). No disclosures were reported by the other authors.

Authors' Contributions

K.E. Miller: Formal analysis, writing—original draft. **K.A. Cassady:** Conceptualization, resources, formal analysis, supervision, methodology, writing—original draft. **J.C. Roth:** Formal analysis. **J. Clements:** Project administration. **K.M. Schieffer:** Formal analysis. **K. Leraas:** Project administration. **A.R. Miller:** Formal analysis. **N. Prasad:** Formal analysis. **J.W. Leavenworth:** Formal analysis. **I.B. Aban:** Formal analysis. **R.J. Whitley:** Supervision, funding acquisition. **G.Y. Gillespie:** Supervision, funding acquisition. **E.R. Mardis:** Supervision, writing—original draft. **J.M. Markert:** Conceptualization, resources, supervision, funding acquisition, investigation, methodology, writing—original draft.

Acknowledgments

This work was supported by grants NIH NCI R01-CA217179 (to J.M. Markert and G.Y. Gillespie), NIH NCI R01-CA222903 (to J.M. Markert and K.A. Cassady), and NIH NCI U54-CA232561 (to E.R. Mardis and K.A. Cassady). K.E. Miller and E.R. Mardis were supported by the Nationwide Insurance Innovation Fund.

The publication costs of this article were defrayed in part by the payment of publication fees. Therefore, and solely to indicate this fact, this article is hereby marked “advertisement” in accordance with 18 USC section 1734.

Note

Supplementary data for this article are available at Clinical Cancer Research Online (<http://clincancerres.aacrjournals.org/>).

Received July 20, 2021; revised September 29, 2021; accepted November 22, 2021; published first February 1, 2022.

References

- Stupp R, Mason WP, van den Bent MJ, Weller M, Fisher B, Taphoorn MJ, et al. Radiotherapy plus concomitant and adjuvant temozolomide for glioblastoma. *N Engl J Med* 2005;352:987–96.
- Zhao YH, Wang ZF, Pan ZY, Peus D, Delgado-Fernandez J, Pallud J, et al. A meta-analysis of survival outcomes following reoperation in recurrent glioblastoma: time to consider the timing of reoperation. *Front Neurol* 2019;10:286.
- James CD, He J, Carlbom E, Nordenskjold M, Cavenee WK, Collins VP. Chromosome 9 deletion mapping reveals interferon alpha and interferon beta-1 gene deletions in human glial tumors. *Cancer Res* 1991;51:1684–8.
- Kohanbash G, McKaveney K, Sakaki M, Ueda R, Mintz AH, Amankulor N, et al. GM-CSF promotes the immunosuppressive activity of glioma-infiltrating myeloid cells through interleukin-4 receptor-alpha. *Cancer Res* 2013;73:6413–23.
- Miyakoshi J, Dobler KD, Allalunis-Turner J, McKean JD, Petruk K, Allen PB, et al. Absence of IFNA and IFNB genes from human malignant glioma cell lines and lack of correlation with cellular sensitivity to interferons. *Cancer Res* 1990;50:278–83.
- Kennedy BC, Maier LM, D'Amico R, Mandigo CE, Fontana EJ, Waziri A, et al. Dynamics of central and peripheral immunomodulation in a murine glioma model. *BMC Immunol* 2009;10:11.
- Cassady KA, Haworth KB, Jackson J, Markert JM, Cripe TP. To infection and beyond: the multi-pronged anti-cancer mechanisms of oncolytic viruses. *Viruses* 2016;8:43.
- Behnan J, Finocchiaro G, Hanna G. The landscape of the mesenchymal signature in brain tumours. *Brain* 2019;142:847–66.
- Wang Q, Hu B, Hu X, Kim H, Squatrito M, Scarpace L, et al. Tumor evolution of glioma-intrinsic gene expression subtypes associates with immunological changes in the microenvironment. *Cancer Cell* 2017;32:42–56.
- Markert JM, Gillespie GY, Weichselbaum RR, Roizman B, Whitley RJ. Genetically engineered HSV in the treatment of glioma: a review. *Rev Med Virol* 2000;10:17–30.
- Markert JM, Liechty PG, Wang W, Gaston S, Braz E, Karrasch M, et al. Phase Ib trial of mutant herpes simplex virus G207 inoculated pre-and post-tumor resection for recurrent GBM. *Mol Ther* 2009;17:199–207.
- Markert JM, Razdan SN, Kuo HC, Cantor A, Knoll A, Karrasch M, et al. A phase I trial of oncolytic HSV-1, G207, given in combination with radiation for recurrent GBM demonstrates safety and radiographic responses. *Mol Ther* 2014;22:1048–55.
- Martuza RL, Malick A, Markert JM, Ruffner KL, Coen DM. Experimental therapy of human glioma by means of a genetically engineered virus mutant. *Science* 1991;252:854–6.
- Patro R, Duggal G, Love MI, Irizarry RA, Kingsford C. Salmon provides fast and bias-aware quantification of transcript expression. *Nat Methods* 2017;14:417–9.
- Soneson C, Love MI, Robinson MD. Differential analyses for RNA-seq: transcript-level estimates improve gene-level inferences. *F1000Res* 2015;4:1521.
- Zerbino DR, Achuthan P, Akanni W, Amode MR, Barrell D, Bhari J, et al. Ensembl 2018. *Nucleic Acids Res* 2018;46:D754–D61.
- Wickham H. *ggplot2: elegant graphics for data analysis*. 2nd ed. Cham: Springer International Publishing; 2016.
- Newman AM, Liu CL, Green MR, Gentles AJ, Feng W, Xu Y, et al. Robust enumeration of cell subsets from tissue expression profiles. *Nat Methods* 2015;12:453–7.
- Love MI, Huber W, Anders S. Moderated estimation of fold change and dispersion for RNA-seq data with DESeq2. *Genome Biol* 2014;15:550.
- Dennis G Jr, Sherman BT, Hosack DA, Yang J, Gao W, Lane HC, et al. DAVID: Database for annotation, visualization, and integrated discovery. *Genome Biol* 2003;4:P3.
- Danaher P, Warren S, Dennis L, D'Amico L, White A, Disis ML, et al. Gene expression markers of tumor infiltrating leukocytes. *J Immunother Cancer* 2017;5:18.
- Li T, Fu J, Zeng Z, Cohen D, Li J, Chen Q, et al. TIMER2.0 for analysis of tumor-infiltrating immune cells. *Nucleic Acids Res* 2020;48:W509–W14.
- Aran D, Hu Z, Butte AJ. xCell: digitally portraying the tissue cellular heterogeneity landscape. *Genome Biol* 2017;18:220.
- Finotello F, Mayer C, Plattner C, Laschober G, Rieder D, Hackl H, et al. Molecular and pharmacological modulators of the tumor immune contexture revealed by deconvolution of RNA-seq data. *Genome Med* 2019;11:34.
- Markert JM, Medlock MD, Rabkin SD, Gillespie GY, Todo T, Hunter WD, et al. Conditionally replicating herpes simplex virus mutant, G207 for the treatment of malignant glioma: results of a phase I trial. *Gene Ther* 2000;7:867–74.
- Leddon JL, Chen CY, Currier MA, Wang PY, Jung FA, Denton NL, et al. Oncolytic HSV virotherapy in murine sarcomas differentially triggers an anti-tumor T-cell response in the absence of virus permissivity. *Molecular therapy oncolytics* 2015;1:14010.
- Ghonime MG, Jackson J, Shah A, Roth J, Li M, Saunders U, et al. Chimeric HCMV/HSV-1 and Deltagamma134.5 oncolytic herpes simplex virus elicit immune mediated antiglioma effect and antitumor memory. *Transl Oncol* 2018;11:86–93.
- Saha D, Martuza RL, Rabkin SD. Macrophage polarization contributes to glioblastoma eradication by combination immunovirotherapy and immune checkpoint blockade. *Cancer Cell* 2017;32:253–67.
- Kurozumi K, Hardcastle J, Thakur R, Yang M, Christoforidis G, Fulci G, et al. Effect of tumor microenvironment modulation on the efficacy of oncolytic virus therapy. *J Natl Cancer Inst* 2007;99:1768–81.
- Chen CY, Wang PY, Hutzen B, Sprague L, Swain HM, Love JK, et al. Cooperation of oncolytic herpes virotherapy and PD-1 blockade in murine rhabdomyosarcoma models. *Sci Rep* 2017;7:2396.
- Currier JR, Galley LM, Wenschuh H, Morafo V, Ratto-Kim S, Gray CM, et al. Peptide impurities in commercial synthetic peptides and their implications for vaccine trial assessment. *Clin Vaccine Immunol* 2008;15:267–76.
- Fulci G, Breyman L, Gianni D, Kurozumi K, Rhee SS, Yu J, et al. Cyclophosphamide enhances glioma virotherapy by inhibiting innate immune responses. *Proc Natl Acad Sci U S A* 2006;103:12873–8.
- Friedman A, Tian JP, Fulci G, Chiocca EA, Wang J. Glioma virotherapy: effects of innate immune suppression and increased viral replication capacity. *Cancer Res* 2006;66:2314–9.
- Wakimoto H, Johnson PR, Knipe DM, Chiocca EA. Effects of innate immunity on herpes simplex virus and its ability to kill tumor cells. *Gene Ther* 2003;10:983–90.
- Gentles AJ, Newman AM, Liu CL, Bratman SV, Feng W, Kim D, et al. The prognostic landscape of genes and infiltrating immune cells across human cancers. *Nat Med* 2015;21:938–45.
- Schalper KA, Rodriguez-Ruiz ME, Diez-Valle R, Lopez-Janeiro A, Porciuncula A, Idoate MA, et al. Neoadjuvant nivolumab modifies the tumor immune microenvironment in resectable glioblastoma. *Nat Med* 2019;25:470–6.
- Cloughesy TF, Mochizuki AY, Orpilla JR, Hugo W, Lee AH, Davidson TB, et al. Neoadjuvant anti-PD-1 immunotherapy promotes a survival benefit with intratumoral and systemic immune responses in recurrent glioblastoma. *Nat Med* 2019;25:477–86.
- Friedman GK, Johnston JM, Bag AK, Bernstock JD, Li R, Aban I, et al. Oncolytic HSV-1 G207 immunovirotherapy for pediatric high-grade gliomas. *N Engl J Med* 2021;384:1613–22.